SAE 2007-24-0084

Model of a Supercharged Diesel Engine with High and Low-Pressure EGR as Part of an NMPC for ECU Implementation

Victor Gheorghiu
Hamburg University of Applied Sciences, Germany

Dietmar Ueberschär
Darmstadt University of Applied Sciences, Germany

Volker Müller and **Ralf Christmann**
BorgWarner Turbo Systems GmbH, Kirchheimbolanden, Germany

ABSTRACT

The paper focuses on a system and an appropriate controller concept for advanced air management of a turbocharged passenger car diesel engine. The proposed air management system consists of a VTG turbocharger and two separate Exhaust Gas Recirculation (EGR) loops, a cooled or non-cooled high-pressure EGR (HP EGR) and a cooled low-pressure EGR (LP EGR) loop. In the LP EGR loop, the exhaust gas leaving the particulate filter is mixed with fresh air just in front of the compressor inlet.

A main model (MM) was created in Simulink to design a Nonlinear Model-based Predictive Controller (NMPC). This model is mainly founded on physical equations, allowing easy adaptation to various systems. MM is a detailed model which was developed first and which is also used for software-in-the-loop (SIL) tests of the controller with the simulated engine.

At the beginning of the diesel engine test stage, stationary measurements were conducted to examine the influence of variations of the EGR rate, boost pressure, fresh air mass, etc. These tests were carried out in an open loop without an integrated controller for the air management system. The results were used to optimize the Simulink models.

As to the controller concept, a model-based predictive approach is briefly presented which uses a simplified simulation model (a reduced version of a more detailed MM) with real-time capability of the complete air path for providing the system states. For the prediction, an additional, simplified model of the engine's air path system with real-time capability is used.

In this paper the main emphasis is on the modeling and the building of the SIL-environment for developing and testing the NMPC. In addition, the controller structure and simulation and measurement results of steady and unsteady tests are presented and analyzed.

INTRODUCTION

NO_x and PM emissions represent the most critical emissions of diesel engines. At present, diesel engines are marketed which comply with Euro 4 and 5 standards, some of the engines even without a diesel particulate filter (DPF). Because of the significant reduction of permissible PM emissions in the transition from Euro 4 to Euro 5 specifications, meeting the future emission standards without integrating cost-intensive after-treatment systems will represent a major challenge. NO_x emissions increase dramatically when the in-cylinder temperature during combustion and the air-fuel ratio (AFR) increase, whereas PM emissions increase otherwise. Generation of NO_x and PM is a local phenomenon, so the local AFR and temperature at each point of the cylinder are of relevance to the generation of these emissions. The known basic interrelationship between NO_x and PM emissions necessitates that any modification of the combustion toward lower NO_x emissions produces higher PM emissions and vice versa.

Many emissions occur during transients, e.g. during acceleration phases which cause peak PM emissions due to insufficient fresh mass air flow supply required for increased fuel injection. During acceleration, the fresh air mass flow does not follow immediately because of the inertia of the air volumes between the air cleaner and the intake manifold. Furthermore, the turbocharger is the most critical part, as it needs to speed up first to generate a higher air mass flow and satisfy the increasing demand for boost pressure.

EGR is used to reduce NO_x emissions. Ideally, the recirculated exhaust gas may be regarded as an inert gas. In

a diesel engine the exhaust gas still contains some oxygen, but compared to the system's fresh air concentration, its oxygen concentration is much lower. Hence, using the EGR to replace part of the fresh air mass with exhaust gas will cause a lower oxygen concentration inside the cylinder. This lack of oxygen leads to reduced NO_x production. The thermal capacity of exhaust gas is higher than that of fresh air (as it contains much more CO_2 and water). This results in lower temperature levels during combustion and, as a consequence, lowers NO_x emissions. Additional cooling of the EGR outside the cylinder helps to decrease this temperature further. The cooling of EGR in the classic configuration with HP EGR loop (by means of the EGR Cooler, top in Fig. 1) is less efficient than the double cooling of LP EGR loop (by means of EGR- and Intercooler, bottom in Fig. 1) of the new configuration.

On the other hand, the boost pressure needs to be increased to reach the target AFR and therefore to avoid higher PM emissions.

To control boost pressure and fresh air mass flow, it is important to reach their required values as accurately and – to reduce emissions during transients – as quickly as possible. Therefore, any improvement of the emission behavior during transients highlights the control concept, thus becoming one of the most important factors in this context. Due to the fact that DPF will become a standard component in future applications, the main focus should be placed on NO_x reduction. The objective is to decrease the scope of required NO_x after-treatment or, if possible, to avoid it completely.

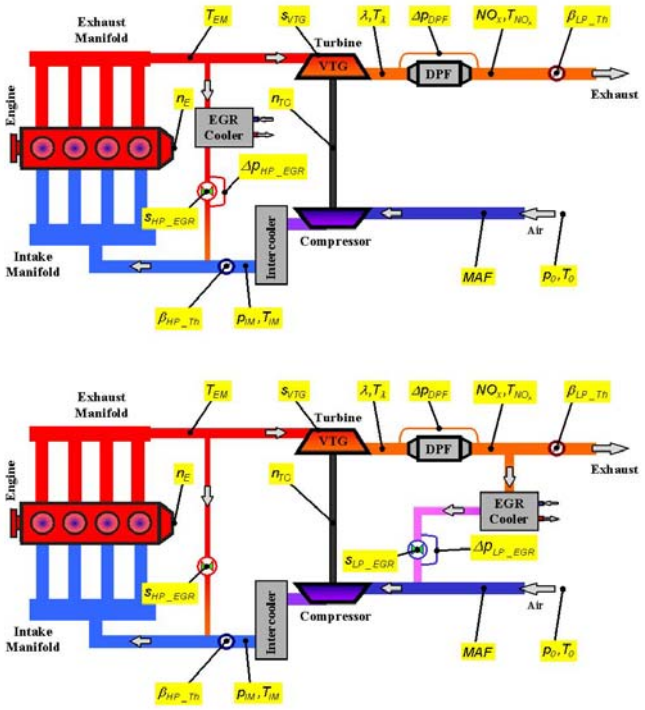

Fig. 1: Classic (top) and new (bottom) system configurations with sensors and actuators

SYSTEM CONFIGURATION

ENGINE CONFIGURATION AND TEST PROCEDURE

For the engine test and simulation stage, a mass-produced DI diesel engine passenger car was used [1], [2]. The air path configuration of this engine met conventional standards, i.e. it was equipped with a high-pressure cooled EGR and pneumatic actuators for the VTG and EGR (top configuration in Fig. 1). First, the engine was tested in its baseline configuration on the engine test bed. After that a new hardware configuration was selected and set up on the dynamometer. Steady-state tests were performed on the dynamometer in the new engine configuration (bottom in Fig. 1). Then, its transient behavior was examined by conducting load steps, first with recalibrated baseline control equipment, i.e. the current mass-produced control system from the ECU which was recalibrated to drive the new (electrical) actuators. The impact of the new system configuration on emissions was analyzed on the basis of this data. Finally, it was planned to repeat the load steps applying the newly developed control strategy.

NMPC IMPLEMENTATION

The new controller uses a model-based predictive approach (NMPC) to determine the subsequent required actuator positions. For the prediction, a model of the engine's air path system with real-time capability is applied. This model is a reduced version of a more detailed model **Model_E** which was developed first and which is also used for software-in-the-loop (SIL) tests of the controller (see below).

The **Model_J** of the NMPC developed for this real time application contains an observer, a predictor and an optimization algorithm (Fig. 2).

The observer model, **Model_S**, uses all available sensor signals to calculate all unmeasured and consequently unknown current states of the system in real time.

The predictor model, named **Model_G,** has no sensor inputs, as it only predicts the future horizon (no sensor signals are available for the future). **Model_G** is stimulated with new actuator positions delivered by the optimization algorithm **J** and estimates the engine's response in the future.

The optimization algorithm **J** judges all estimations by calculating a cost function for each simulated actuator position set [1], [2]. Both the observer (**Model_S**) and the predictor (**Model_G**) are model-based and both models are derived from the detailed engine model **Model_E**.

Fig. 2 shows the integration of the NMPC as **Model_J** in parallel with a mass-produced ECU for engine control on the dynamometer. For this implementation, some ECU functions need to be bypassed. The development ECU

used here still controls most of the engine functions, e.g. injection timing. Sensor signals and other ECU variables may be read out via the ETK interface of the ECU. An ASCET ES1000 real-time system is used for the bypass functionality. The ASCET system captures sensor signals via the ETK interface and via additional I/O ports (for additional sensors not used in the standard ECU). The Simulink controller model is implemented on the ASCET system to carry out all previously simulated controller functions. The actuators are operated via the D/A or PWM output drivers of the ASCET system.

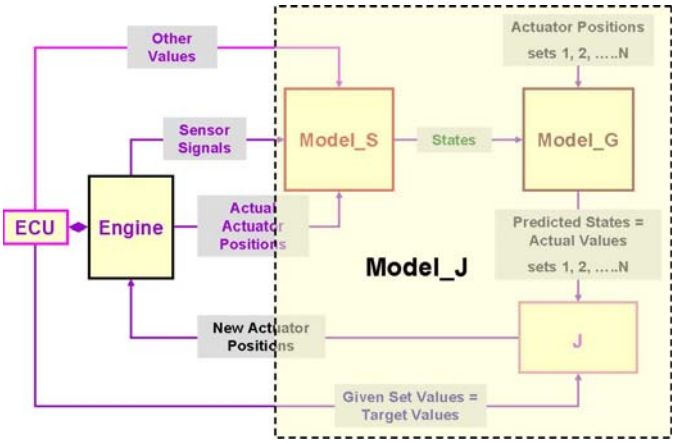

Fig. 2: Combining the NMPC with a mass-produced ECU

SIL ENVIRONMENT FOR NMPC DEVELOPMENT

To develop and pre-calibrate this NMPC, a SIL environment was created. In this SIL environment, the simulation model **Model_E** replaces the engine and the mass-produced ECU (as shown in Fig. 3). To implement this SIL environment of **Model_J** (which must work in real-time within a sampling time of 1 msec in ECU) into Simulink, a multi-rate application needs to be realized, since **Model_E** uses a much shorter sampling time (here 5 µsec) for numeric stability and accuracy reasons (see Fig. 4).

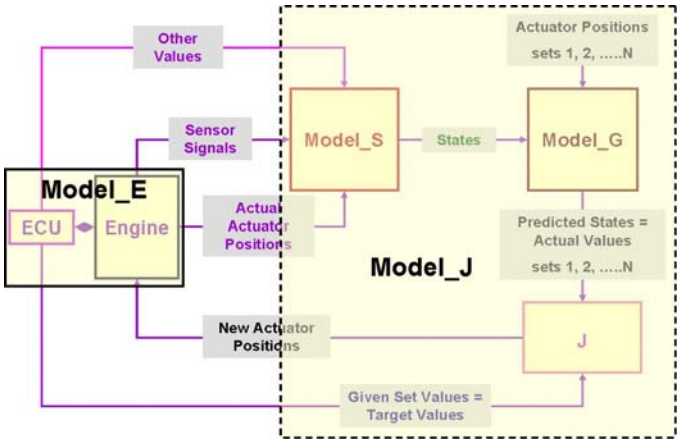

Fig. 3: SIL environment for NMPC development

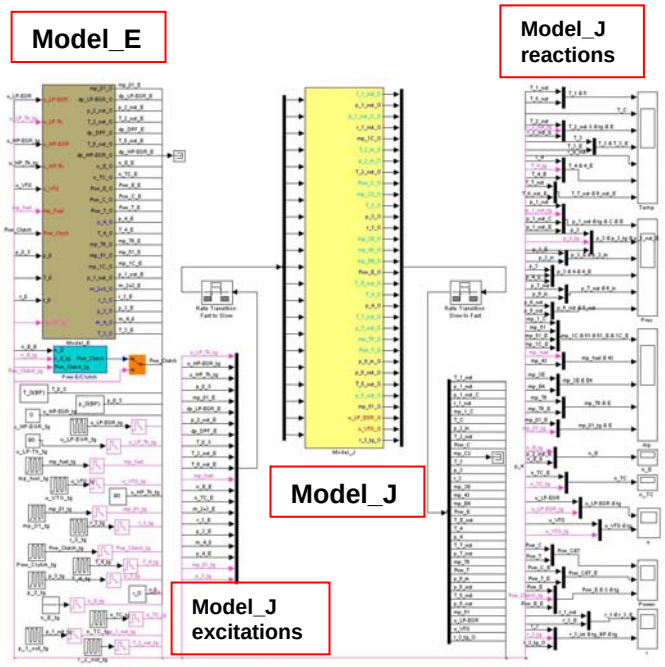

Fig. 4: Simulink implementation of the SIL environment for NMPC (Model_J) as multi rate application (zoomed)

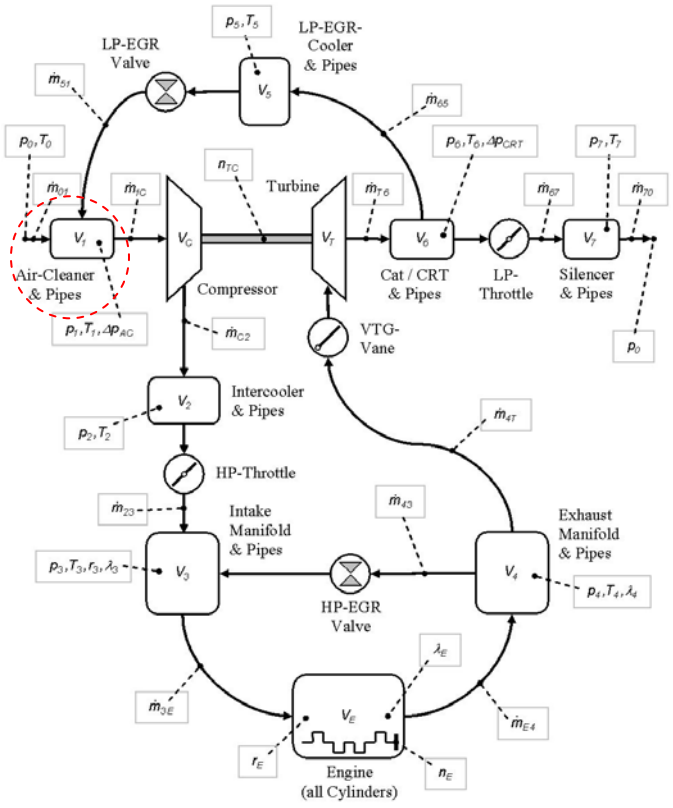

Fig. 5: Schematic representation of Model_E. Selected is here the Air-Cleaner Volume (zoomed)

SIMULINK ENGINE MODELS

The detailed engine model, named **Model_E** here, is developed in part on a physical basis (e.g. for manifolds and all other volumes) and in part on an empirical basis (e.g. for the turbocharger (TC) and cylinder). Fig. 5 shows all modeled physical components as well as the interaction variables between them. Each physical component has a Simulink representation with its own block as shown in Fig. 6.

VOLUME (PLENUM) SUBMODEL

All volumes are described by means of the differential balance equations for the mass of the gas mixture (1), the EGR rate (2) and the energy (3), i.e. by means of the filling and emptying method [3], [4], [5]. The air mass of the entire system, treated as ideal gas, is considered here concentrated only in these volumes.

$$\frac{d}{dt}m = \sum_i m'_i - \sum_j m'_j \qquad (1)$$

$$\frac{d}{dt}r_k = \frac{1}{m}\cdot\sum_i\left[m'_i\cdot\left(r_{k_i} - r_k\right)\right] \quad \text{where} \quad r_k = \frac{m_k}{m} \qquad (2)$$

$$\frac{d}{dt}T = \frac{1}{m}\cdot\left[\frac{Q'}{c°_v} + \kappa\cdot\left[\sum_i\left(m'_i\cdot T_i\right) - T\cdot\sum_j m'_j\right] - T\cdot\frac{d}{dt}m\right] \qquad (3)$$

with:

States in the actual volume

m	mass of the gas mixture
r_k	mass fraction of gas component k (e.g. EGR)
T	temperature

Exchanged quantities

m'_i	input mass flow
m'_j	output mass flow
Q'	heat flow

Other

t	time
$c°_v$	isochore thermal capacity of gas mixture
κ	isentropic exponent

The mass flow rates between these volumes are regarded here as **isothermal**, since this provides a more realistic description of the flow process behavior (i.e. closer than an isentropic flow as in [3], [4], [5] and many other publications assumed). In this way the isentropic flow discharge coefficients (for the isentropic flow rate correction) are in principle no longer needed. For visualization purposes, the reader may assume the integration of a throttle or a valve between two pipe parts. This system may be considered adiabatic with a steady flow running through the throttle (both assumptions need to be transferred to an isentropic system as well). To demonstrate that the mass and energy balance equations have been considered (see the squared area; the specific kinetic energy of the flow is neglected here for simplicity):

$$\frac{d}{dt}m = m'_{in} - m'_{out}$$

$$\frac{d}{dt}U = Q' + m'_{in}\cdot h_{in} - m'_{out}\cdot h_{out}$$

where steady process implies

a) $\frac{d}{dt}m = 0$ for mass, i.e. $m'_{in} = m'_{out} = m'$

b) $\frac{d}{dt}U = 0$ for internal energy,

and adiabatic system means $Q' = 0$

For the spec. enthalpy results $h_{in} - h_{out} = 0$

which for ideal gas means $T_{in} = T_{out}$ i.e. isothermal.

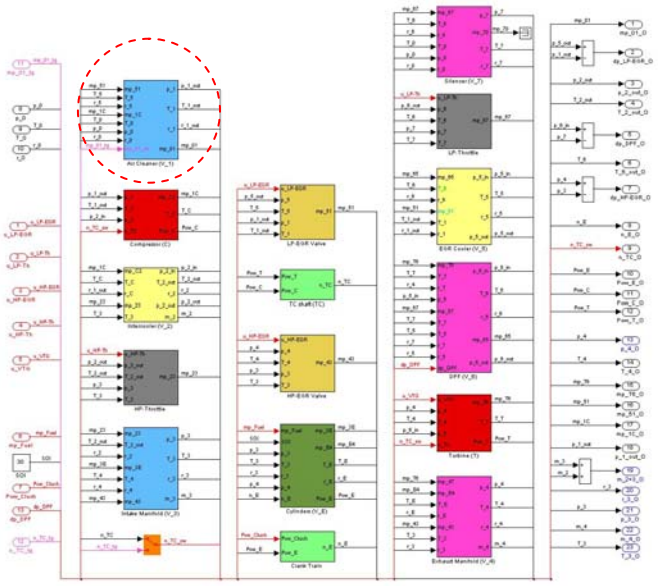

Fig. 6: Simulink representation of **Model_E**. Selected is here the Air-Cleaner Submodel (zoomed)

AIR CLEANER SUBMODEL AS AN EXAMPLE OF MODEL REDUCTION FOR REAL-TIME APPLICATION

To explain the particularity of model reductions from **Model_E** to **Model_S** and from **Model_E** to **Model_G,** the transformations for the air cleaner submodel (see selected blocks from Fig. 5 and 6) are exemplified here. Characteristic here are a) the small pressure differences between atmosphere (index 0), volume V_1 (Air Cleaner) and volume V_5 (LP-EGR Cooler & Pipes), b) the big cross-sections of the pipes and c) the relative reduced capacity of volume V_1. For these reasons the signs of the mass flow rates can change each integration step. As a result, the mass flow rate behavior starts to oscillate widely. The intensity of these oscillations depends

additionally on the sampling time (i.e. integration step) length.

Air Cleaner Submodel of **Model_E**

The inputs of the air cleaner submodel of **Model_E** (see Fig. 7) include:

1. the ambient states,
2. the states of the connecting pipe between the LP EGR valve and the air cleaner (mass flow, temperature and EGR rate), and
3. the mass flow rate sucked from the compressor.

In this submodel, the air mass flow rate mp_01 between atmosphere and volume V_1 is computed and thus the three balance equations (1) to (3) can be integrated as shown in Fig. 7. The air cleaner submodel outputs cover the states and this mass flow rate (fourth output). The flow discharge coefficient (Cd) is calibrated and deduced from dynamometer measurements. Because the sampling time used here is short (5 µs), the oscillations of the mp_01 have only a low intensity and can be neglected.

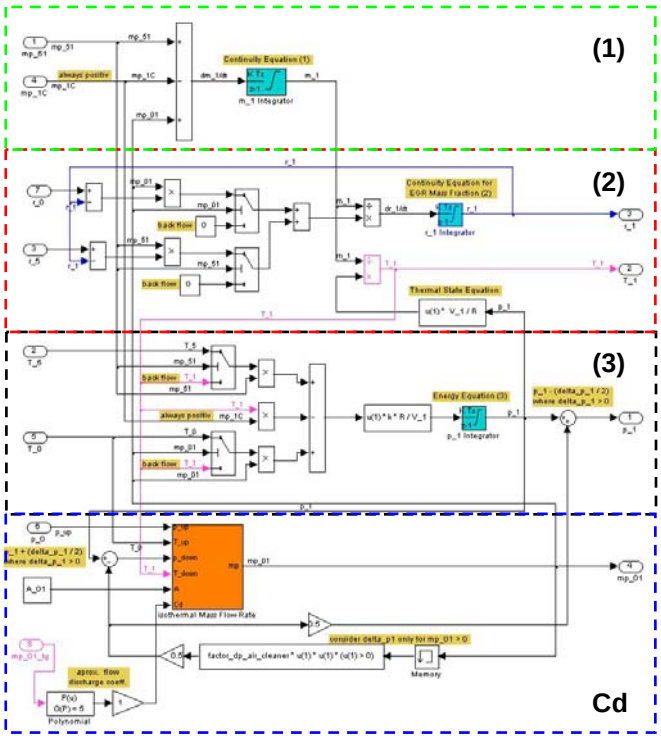

Fig. 7: Air Cleaner submodel from **Model_E** (zoomed)

Air Cleaner Submodel of Observer **Model_S**

The target of the **Model_S** is to provide the current system states for the **Model_G**, i.e. to keep step with the engine (as observer) and to initialize the predictor. **Model_S** works in real-time within a sampling time of 1 msec. In this relatively short time many other tasks must be computed. One of them is, for example, the predictor **Model_G**. On the other hand, all sensor signals (with their specific delays) can be used here. For these reasons significant model reduction from **Model_E** to **Model_S** can and must be carried out here.

As an example, the air cleaner submodel as part of **Model_S** does not need to calculate the air mass flow rate, as it is continuously available as a sensor signal (input 2 and signal mp_01, left selection in Fig. 8). Because of the low dynamic of the filling and emptying processes of the volume V_1, the differential balance equations (1), (2), (3) can be reduced to algebraic functions. In consequence, only steady-state mixing processes for the EGR rate and temperature may be implemented here. By comparing the computed and measured air mass flow rate, the flow discharge coefficient may be calibrated to use as input to **Model_G** (see right selection in Fig. 8). The calculated gas mixture mass flow rate and the other states of this volume are used as initialization states of the predictor **Model_G**.

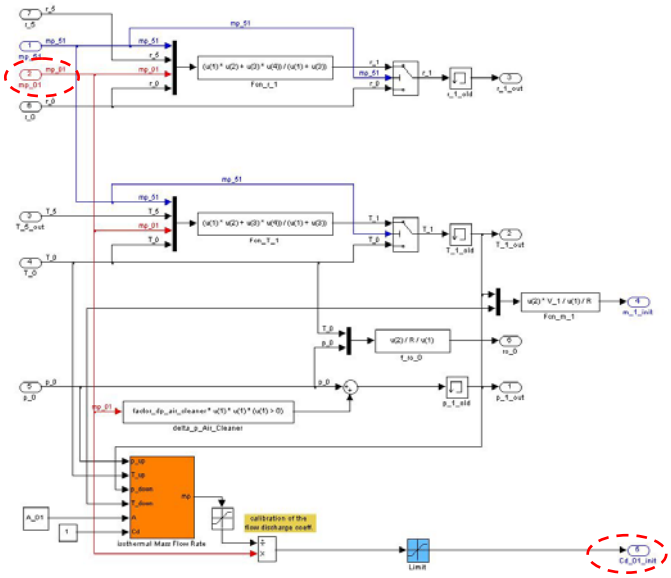

Fig. 8: Air Cleaner submodel from **Model_S** (zoomed)

Air Cleaner Submodel of Predictor **Model_G**

As already mentioned **Model_G** works in real-time in parallel with **Model_S** within a sampling time of 1 msec. The air cleaner submodel used in **Model_G** needs to compute the air mass flow rate because no sensor signals are available during predictions. Since this submodel is expected to sensitively and accurately respond to different actuator settings, the differential balance equations (1), (2) and (3) may no longer be neglected here (see Fig. 9). For this reason no model reduction for **Model_E** can be carried out here.

Two important differences concerning **Model_E** can be identified in Fig. 9:

1. Before starting the predictions for many combinations of EGR-Valves and VTG-Vane settings, all integrators need to be externally reset (red inputs) and initialized (blue inputs) with the states provided by **Model_S** (see right selection for reset input signal in Fig. 9).
2. To prevent the mass flow rate oscillations - as mentioned above - a PT1 controller (in the figure named PT1-filter) is inserted. This measure is needed here because of the relatively large integration time (of 1 msec).

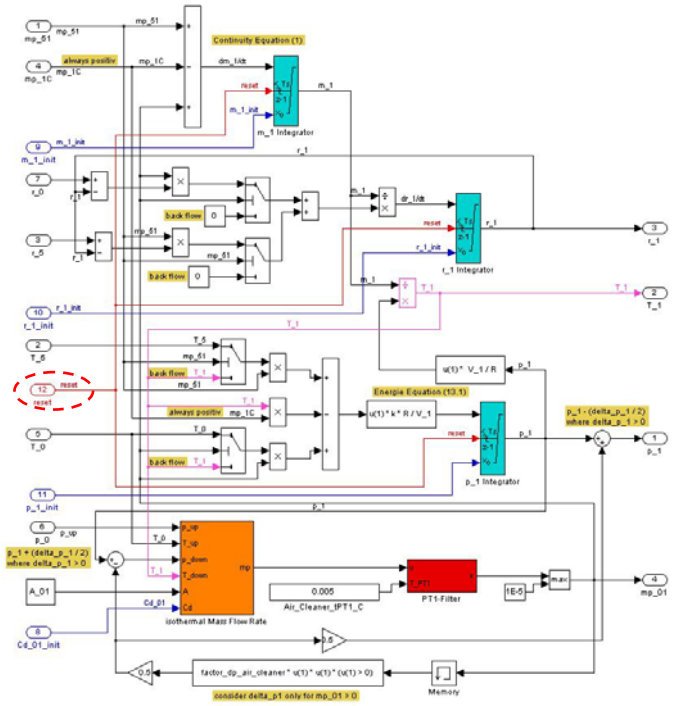

Fig. 9: Air Cleaner submodel from Model_G (zoomed)

TURBOCHARGER (TC) SUBMODELS

The TC maps are processed to eliminate current interpolation difficulties.

Compressor Map

The classic compressor maps (Fig. 10) represent the pressure ratio in relation to the reduced mass flow rate and the isentropic efficiency in relation to the reduced mass flow rate at various TC speeds. If the pressure ratio (from the states of the adjacent volumes) and the TC speed are known and the reduced mass flow is to be specified, two or more solutions may be obtained at higher TC speeds due to the curves' flatness, as shown in the upper map of Fig. 10 with dashed lines. However, this is physically impossible i.e. only one of these two or more solutions can be right.

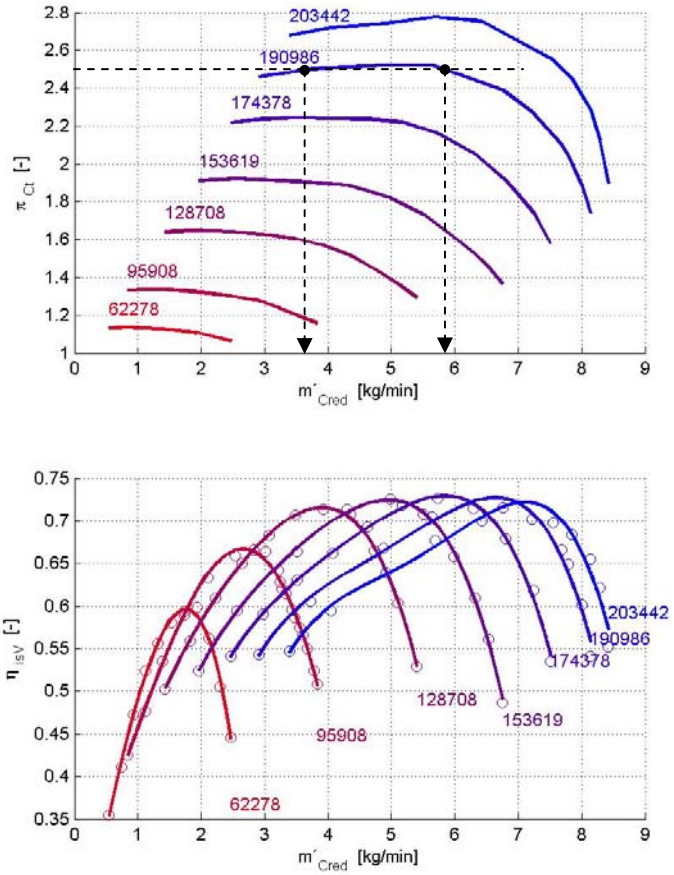

Fig. 10: Classic compressor maps

To avoid such situations, the maps are appropriately processed (i.e. physically) by combining the information of both maps. This results in a new map combination as shown in Fig. 11. The abscissa of the upper map of Fig. 11 signifies in this case the relative increase of the enthalpy (or temperature by constant isentropic exponent) between compressor outlet and inlet. In the squared area, a short demonstration is given; the specific kinetic energy of the flow is neglected here for simplicity.

The isentropic (index s; in Fig. 10 and 11 it is labeled η_{siV}) efficiency of the compressor is defined as

$$\eta_s = \frac{\Delta h_s}{h_{out} - h_{in}}$$

where h is the specific enthalpy before (index in) and after (index out) compressor. The isentropic increase of the gas specific enthalpy across the compressor

$$\Delta h_s = h_{in} \cdot \left(\pi^{\frac{\kappa-1}{\kappa}} - 1 \right)$$

depends on the specific enthalpy in front of, and pressure ratio

$$\pi = \frac{p_{out}}{p_{in}} > 1$$

across, the compressor. The real increase of the gas specific enthalpy related to the specific enthalpy before the compressor

$$\frac{h_{out} - h_{in}}{h_{in}} = \frac{h_{out}}{h_{in}} - 1 = \frac{T_{out}}{T_{in}} - 1$$

can be used as a new abscise. After some operations this results in (referring to both ordinates of the maps in Fig. 10)

$$\frac{h_{out} - h_{in}}{h_{in}} = \frac{\pi^{\frac{\kappa-1}{\kappa}} - 1}{\eta_s}$$

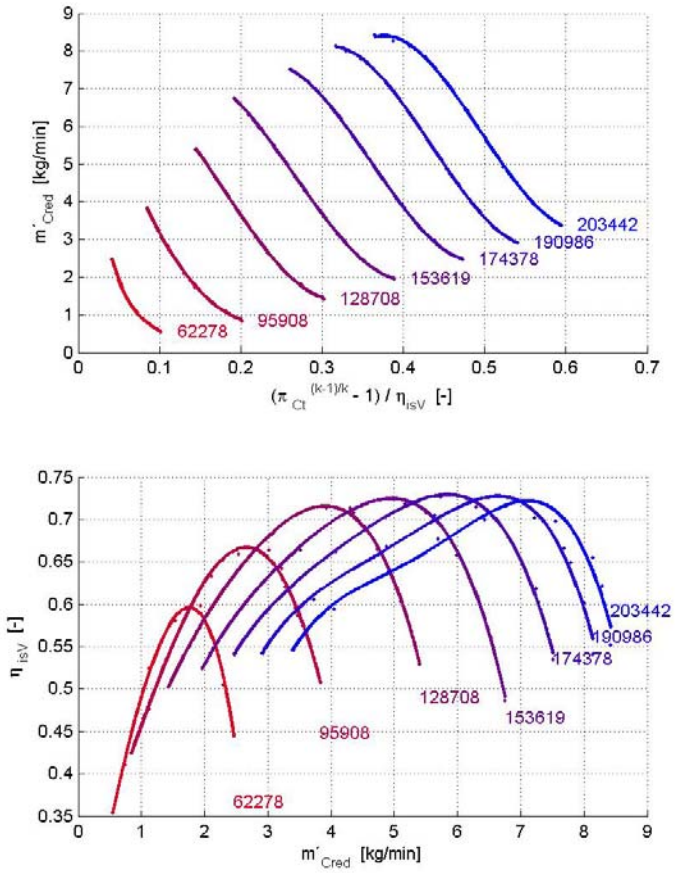

Fig.: 11: Processed compressor maps

The solution can be found iteratively. For example, the isentropic efficiency from the bottom map of Fig. 11 can be found using a known TC speed and the last value of the reduced mass flow rate (i.e. from last integration step). This value together with the pressure ratio allows us, using the upper map, to estimate the new reduced mass flow rate value. One or more iterations may be necessary to achieve the convergence.

Turbine Map

The situation in the turbine is similar, but significantly complicated by the impact of the VTG. The turbine maps of Fig. 12 represent the reduced mass flow rate in relation to the pressure ratio (upper) and the product of isentropic and mechanical efficiency in relation to the reduced pressure ratio (bottom), both with the reduced TC shaft speeds and the VTG position as parameters. Only the bottom map appears relatively complicated because of the fragmented curves.

The problem may be resolved in a similar way to the compressor map. The difficult problem originating in the unsteady and fragmented curves can then be resolved.

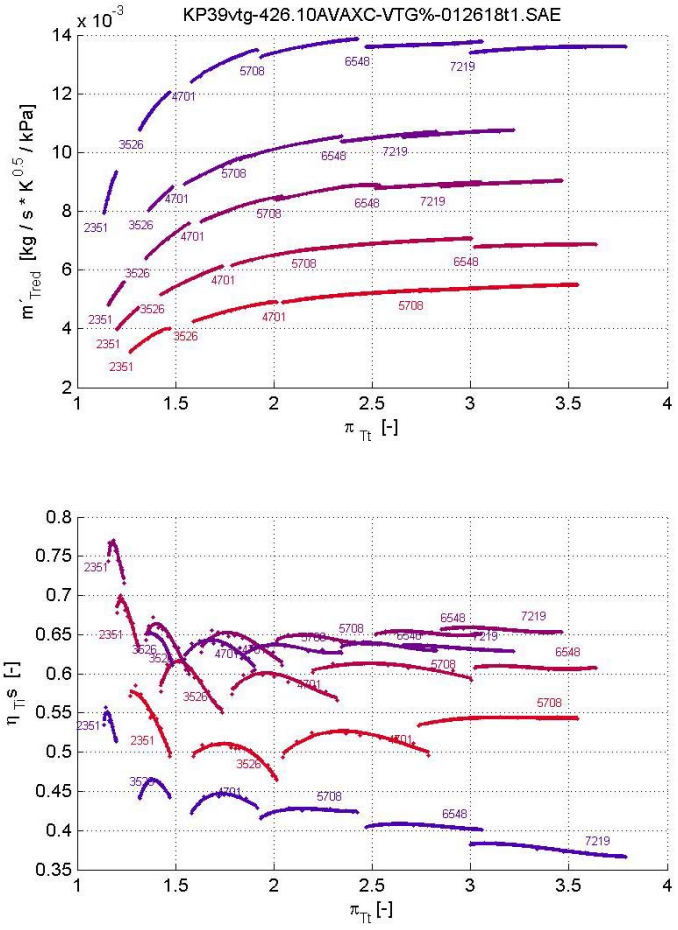

Fig. 12: Classic turbine maps

The ordinate of the lower map in Fig. 13 signifies in this case the relative decrease in the total enthalpy (or total temperature by constant isentropic exponent) between turbine outlet and inlet (see the demonstration from the squared area).

The isentropic (index s; in Fig. 12 and 13 it is labeled η_{Tis}) efficiency of the turbine is defined as

$$\eta_s = \frac{h_{in} - h_{out}}{\Delta h_s}$$

where h is the specific enthalpy before (index in) and after (index out) turbine. The isentropic decrease of the exhaust gas specific enthalpy across the turbine

$$\Delta h_s = h_{in.t} \cdot \left(1 - \frac{1}{\pi^{\frac{\kappa-1}{\kappa}}}\right)$$

depends on the total (add. index t) specific enthalpy before turbine

$$h_{in.t} = c°_p \cdot T_{in} + \frac{c_0^2}{2}$$

and pressure expansion ratio

$$\pi = \frac{p_{in}}{p_{out}} > 1$$

across the turbine, where T is the temperature, $c°_P$ the isobar heat capacity and c_0 the gas flow speed in front of the turbine. After some operations (similar to compressor) it results either in

$$\left(1 - \frac{1}{\pi^{\frac{\kappa-1}{\kappa}}}\right) \cdot \eta_s \cdot \left(1 + \frac{c_0^2}{2 \cdot c°_p \cdot T_{in}}\right) = \frac{T_{in} - T_{out}}{T_{in}} = 1 - \frac{T_{out}}{T_{in}}$$

or by using of the total temperature in front of turbine $T_{in.t}$

$$\left(1 - \frac{1}{\pi^{\frac{\kappa-1}{\kappa}}}\right) \cdot \eta_s + \frac{c_0^2}{2 \cdot c°_p \cdot T_{in}} = \frac{T_{in.t} - T_{out}}{T_{in.t}} = 1 - \frac{T_{out}}{T_{in.t}}$$

The mechanical efficiency of the TC (η_{TCm}) must be included here (multiplied by the isentropic turbine efficiency as shown in Fig. 13) because it cannot be identified separately during TC test bed measurements.

Additionally, the TC speed is no longer a parameter of the maps, i.e. only the VTG vane position still remains as a parameter in this case.

CYLINDER SUBMODEL

The cylinder submodel is partly physical (modeled as plenum) and partly empirical, i.e. it is based on dynamometer measurements carried out solely on mass-produced engines (with mass-produced ECUs).

The cylinder submodel is developed as a **mean values model**, i.e. all its states are not a function of the crank angle. The following states of this submodel need to be determined:

- the per-cycle gas mixture sucked into the cylinders,
- its EGR rate,
- the temperature of the exhaust gas leaving the cylinder and
- the engine power.

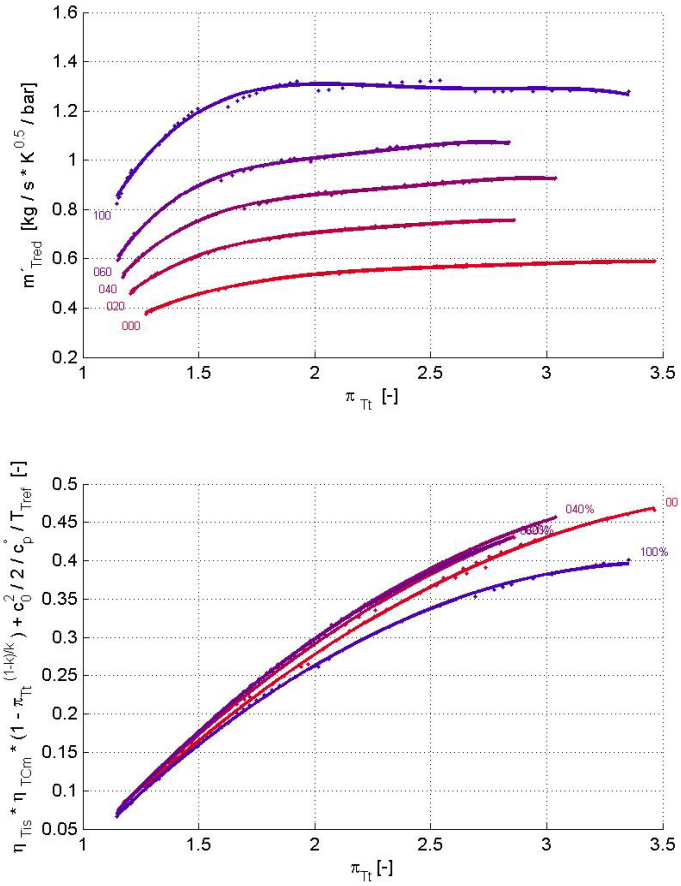

Fig. 13: Processed turbine maps

The following factors were taken into consideration during the development of the cylinder submodel:

1. Since the entire model is projected for real-time operation, no detailed physical model may be used here.
2. The mass flow sucked into the cylinder depends more on density than on the pressure from the intake manifold.
3. The gas mixture of air and EGR from the intake manifold is homogenized.
4. The exhaust gas mass leaving the cylinder is equal to the sum of the sucked gas mixture mass and fuel mass (steady-state gas exchange process).
5. The exhaust gas temperature and the engine power depend on:
   - the filled cylinder (volume) and therefore on the density of the gas in the intake manifold
   - the engine speed,
   - the air-fuel-ratio (lambda),

- the EGR rate into the cylinder and
- the start of injection (SOI).

RESULTS OF SIL SIMULATIONS AND OF TESTS ON ENGINE TEST BENCH

Fig. 14 shows the results of a simulation during a VTG actuator step. The engine was simulated at an operation point of 3000 rpm and 9 bar BMEP.

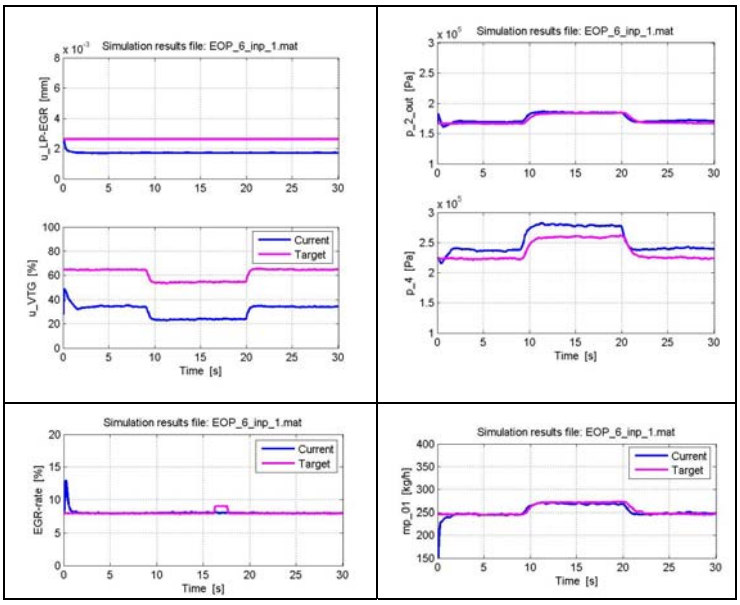

Fig. 14: Simulation results of the engine model during a VTG actuator step

Choosing the targets has a major influence on the performance of this NMPC algorithm. Since the desired values for the air mass flow rate, EGR rate and boost pressure are taken over from the mass-produced ECU, and thus optimized only for HP EGR, they will not fit exactly into the modified engine with an additional low pressure EGR line.

Compared to LP EGR, HP EGR leads to higher intake manifold temperatures. Hence, to reach the same air and EGR mass flow rates, HP EGR requires a higher boost pressure (due to thermal state equation).

Consequently, selecting the boost pressure and the air mass flow rate from a mass-produced ECU with HP EGR as target values will result in an excessive air mass flow rate and a fully uncoordinated EGR rate as shown in Fig. 15. The choice of the boost pressure and EGR rate as targets gives better results but the air mass flow rate remains slightly excessive as shown in Fig. 16.

Regarding the cylinder-filling process, the air and EGR mass flow rates are more important than the boost pressure. The simulation results shown in Fig. 17 confirm this statement.

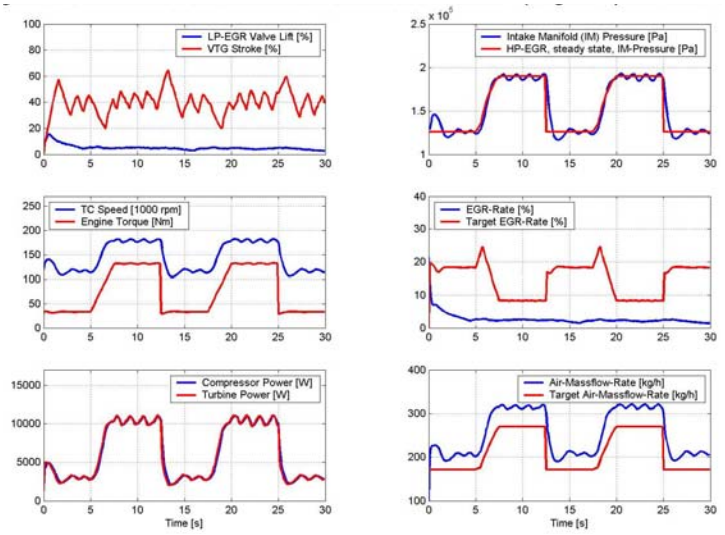

Fig. 15: SIL Test of NMPC; **targets: air mass flow rate and boost pressure**

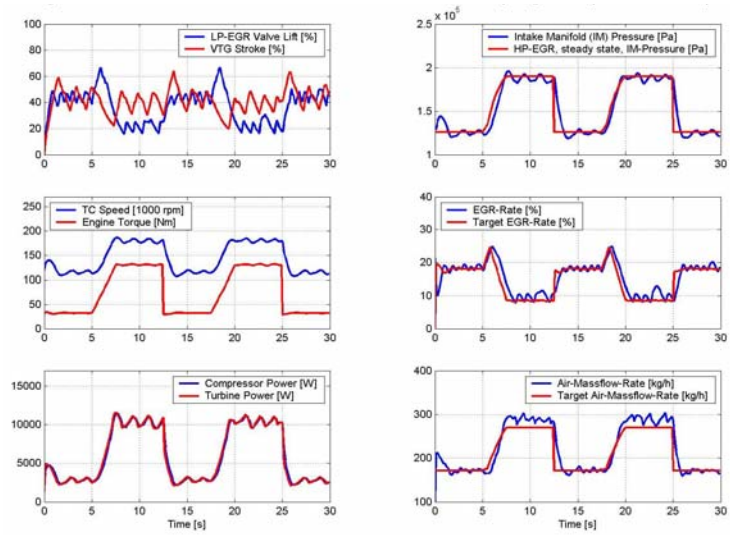

Fig. 16: SIL Test of NMPC; **targets: EGR rate and boost pressure**

These tests reveal that the targets should be chosen taking the changed requirements of the modified hardware into consideration. This renders the development of an NMPC more difficult, as adequate target values are missing when this controller is tested together with the modified engine and its mass-produced ECU on the engine test bench.

After implementation on the NMPC and provision of suitable instrumentation of the LP EGR in the engine, many dynamometer tests were carried out.

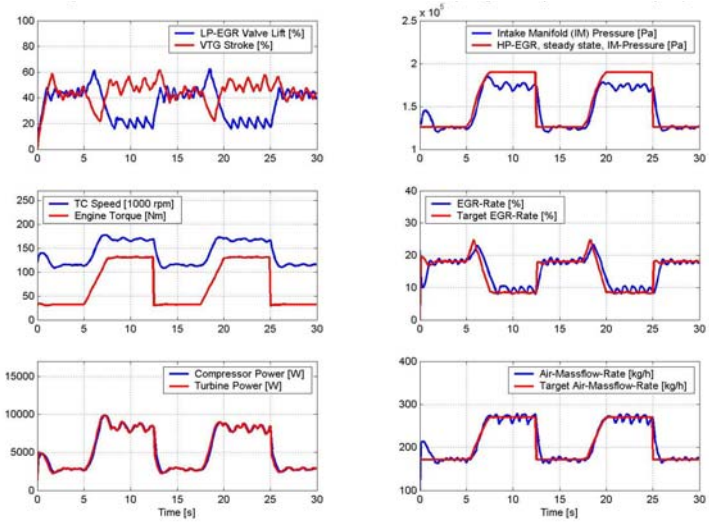

Fig. 17: SIL Test of NMPC; **targets: EGR rate and air mass flow rate**

Fig. 18 shows some first dyno results with this controller. A constant speed load jump was conducted, which is shown in the upper left diagram. In the lower left diagram we can see the actuator positions recorded during this test, the blue line for the VTG and the green line for the LP EGR valve. It is apparent that both actuators are controlled simultaneously. Compared to the simulation, no oscillations occur, but the whole control procedure works very slowly. This can be seen in the diagrams for the control variables boost pressure and fresh air mass flow as shown on the right side, where the air mass flow control is much faster than the boost pressure control.

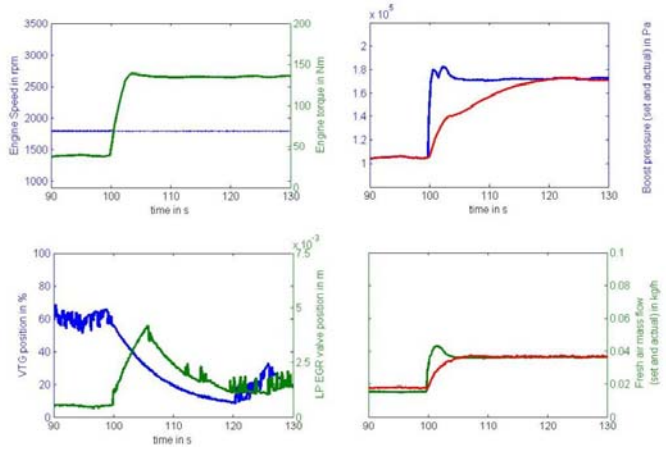

Fig. 18: Engine test bench results of NMPC

In summary, therefore, the controller works stably and shows aperiodic behavior. Of course, major potential for further optimization lies in improving the dynamics. For this, the models for the observer and the predictor can be improved but also the whole controller principle may have to be modified, e.g. by changing the prediction horizon. This can allow a modification of the regressive filter for the new actuator positions which will improve the dynamics of the system. But all these modifications have to take into account the fact that the computing time is limited.

CONCLUSION

The combination of the state-of-the-art HP EGR and an LP EGR would appear to be a system which is capable of complying with the requirements of new emission standards. The benefits of this system can only be realized in combination with a new controller concept. The proposed predictive model-based controller ensures good transient and steady-state control behavior.

The development process for an NMPC controller can be drastically shortened if a SIL environment is built for this purpose. This development strategy permits good comparison of SIL and HIL simulations due to the fact that both methods can be used in parallel without modification of the NMPC controller (i.e. of **Model_J**).

The necessary model reductions for real-time running capability of some submodels of **Model_J** are presented and commented upon.

For the compressor and turbine maps, new processing methods are presented which drastically reduce the interpolation effort and eliminate their uncertainty.

Additionally, further optimizations of the controller concept need to be evaluated and proven in the test runs on the engine test bench. Only the combination of an optimized control strategy and a system approach to the required changes of the hardware would seem to pave the way for making such combined HP and LP EGR systems feasible in subsequent stock production.

ACKNOWLEDGMENTS

This project was funded and directed by BorgWarner Turbo Systems with the support of both universities mentioned. BorgWarner wants to thank all those who supported this project for their excellent work.

REFERENCES

1. Gheorghiu, V. & Müller, V., Christmann, R., Münz, S. (BorgWarner Turbo System GmbH) : *System und regelungskonzept für zukünftige Turbolader-Abgasrückführsysteme für turboaufgeladener Diesel Pkw*, (German) Aufladtechnische Konferenz, Dresden, September 2005 (*.pdf, 0.8 MB)

2. Gheorghiu, V. & Müller, V., Christmann, R., Münz, S. (BorgWarner Turbo System GmbH) : *System Structure and Controller Concept for an Advanced Turbocharger/EGR System for a Turbocharged Passenger Car Diesel Engine*, SAE 2005-01-3888, October 2005, San Antonio, USA (*.pdf, 1.7 MB)

3. Benson, R. S. The Thermodynamic of Gas Dynamics of Intenal Combustion Engines, Claredon Press, Oxford, 1982

4. Heywood, J. B.: Internal Combustion Engine Fundamentals, McGraw Hill, 1988

5. Zinner, K., Supercharging of Internal Combustion Engines, Springer, 1978

CONTACT

Victor GHEORGHIU
Prof. PhD ME
Hamburg University of Applied Sciences
Faculty Technics and Informatics
Dpt. of Mechanical Engineering
Berliner Tor 21
20099 Hamburg, Germany
grg@rzbt.haw-hamburg.de
www.haw-hamburg.de/pers/Gheorghiu/index.html
www.victor-gheorghiu.de

APPENDIX OF ZOOMED FIGURES

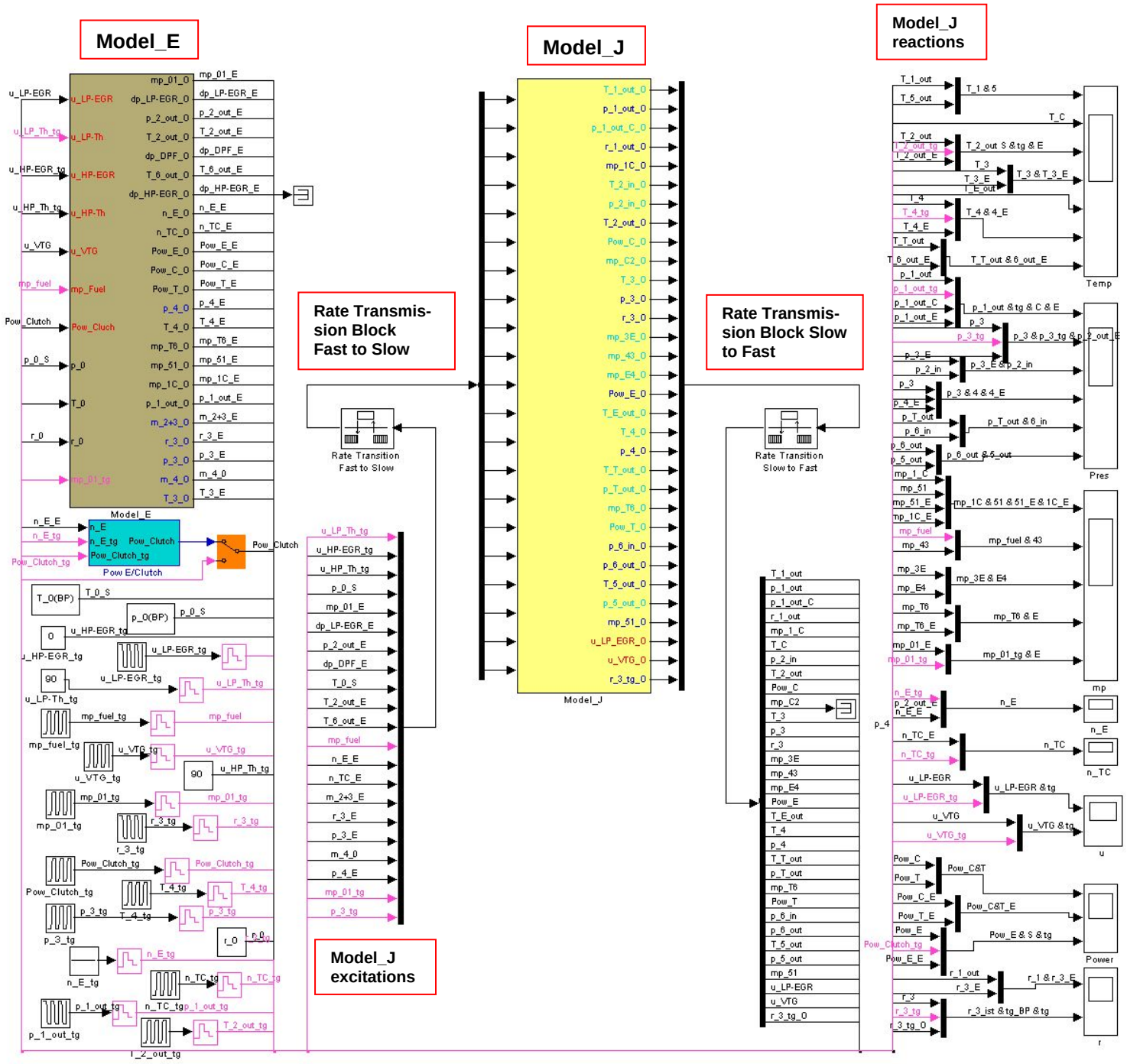

Fig. 4 (zoomed): Simulink implementation of the SIL environment for NMPC (Model_J) as multi rate application (go back)

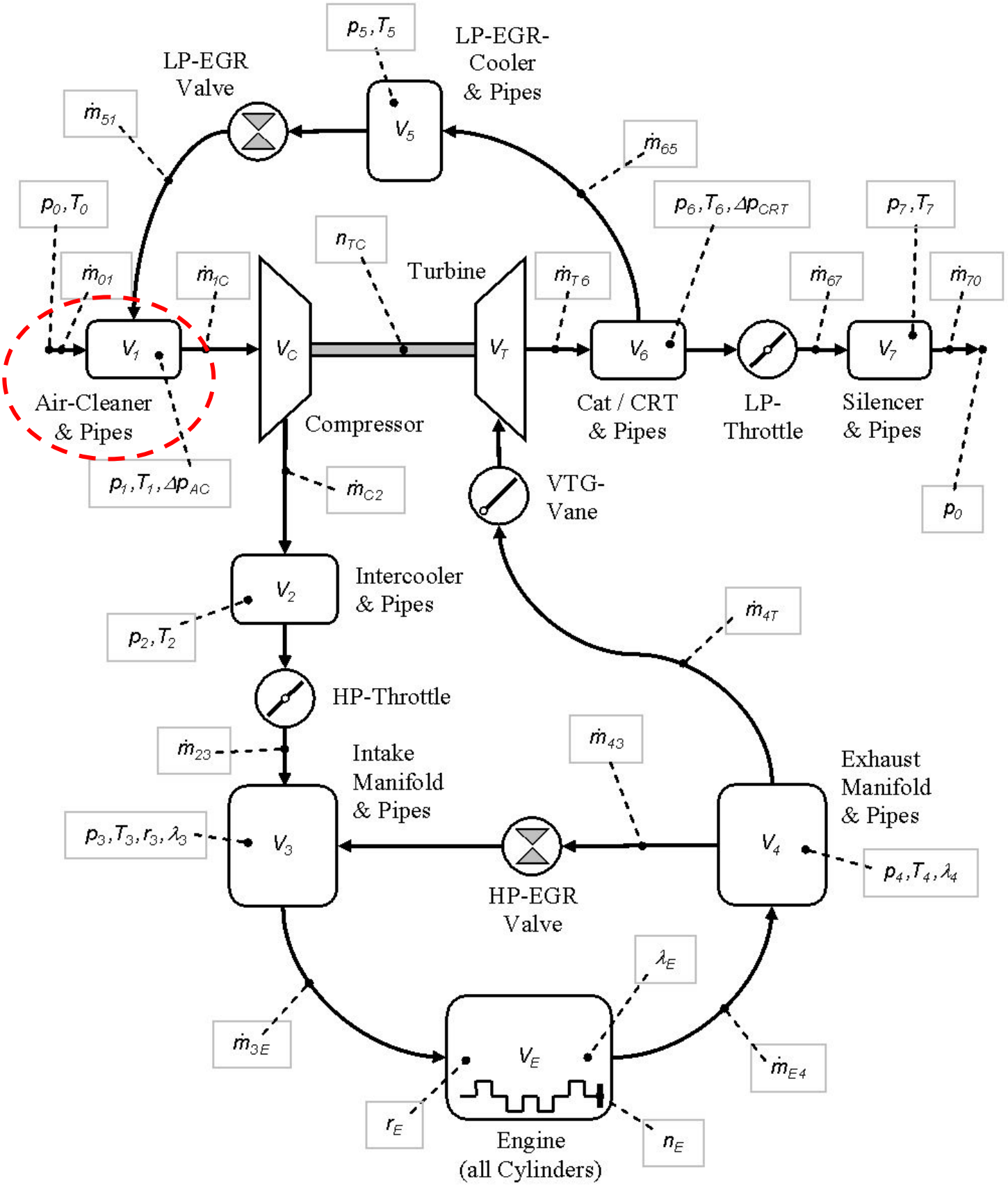

Figure 5 (zoomed): Schematic representation of Model_E. Selected is here the Air-Cleaner Volume (go back)

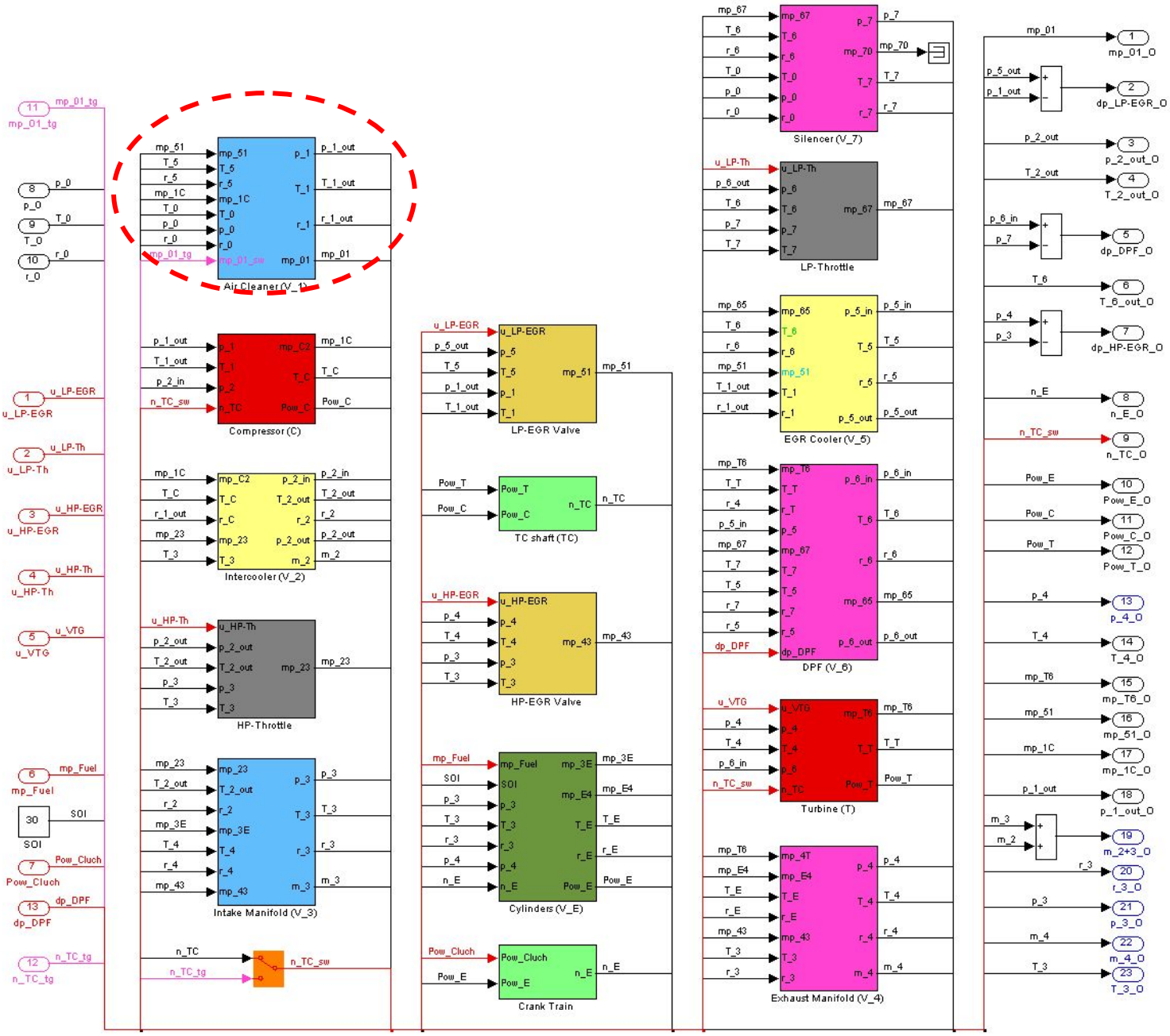

Figure 6 (zoomed): Simulink representation of **Model_E**. Selected is here the Air-Cleaner Submodel (go back)

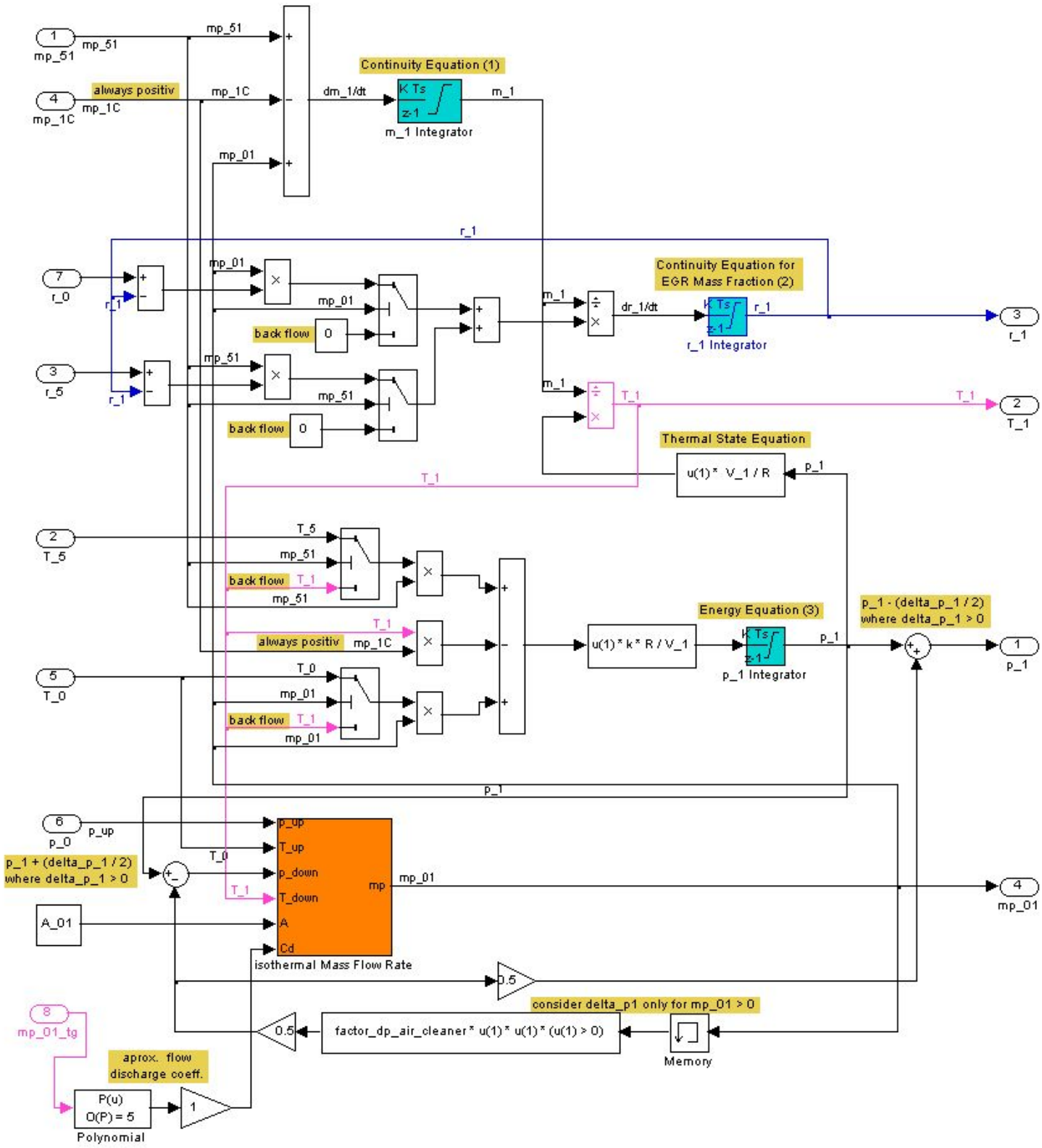

Fig. 7 (zoomed): Air Cleaner submodel from Model_E (go back)

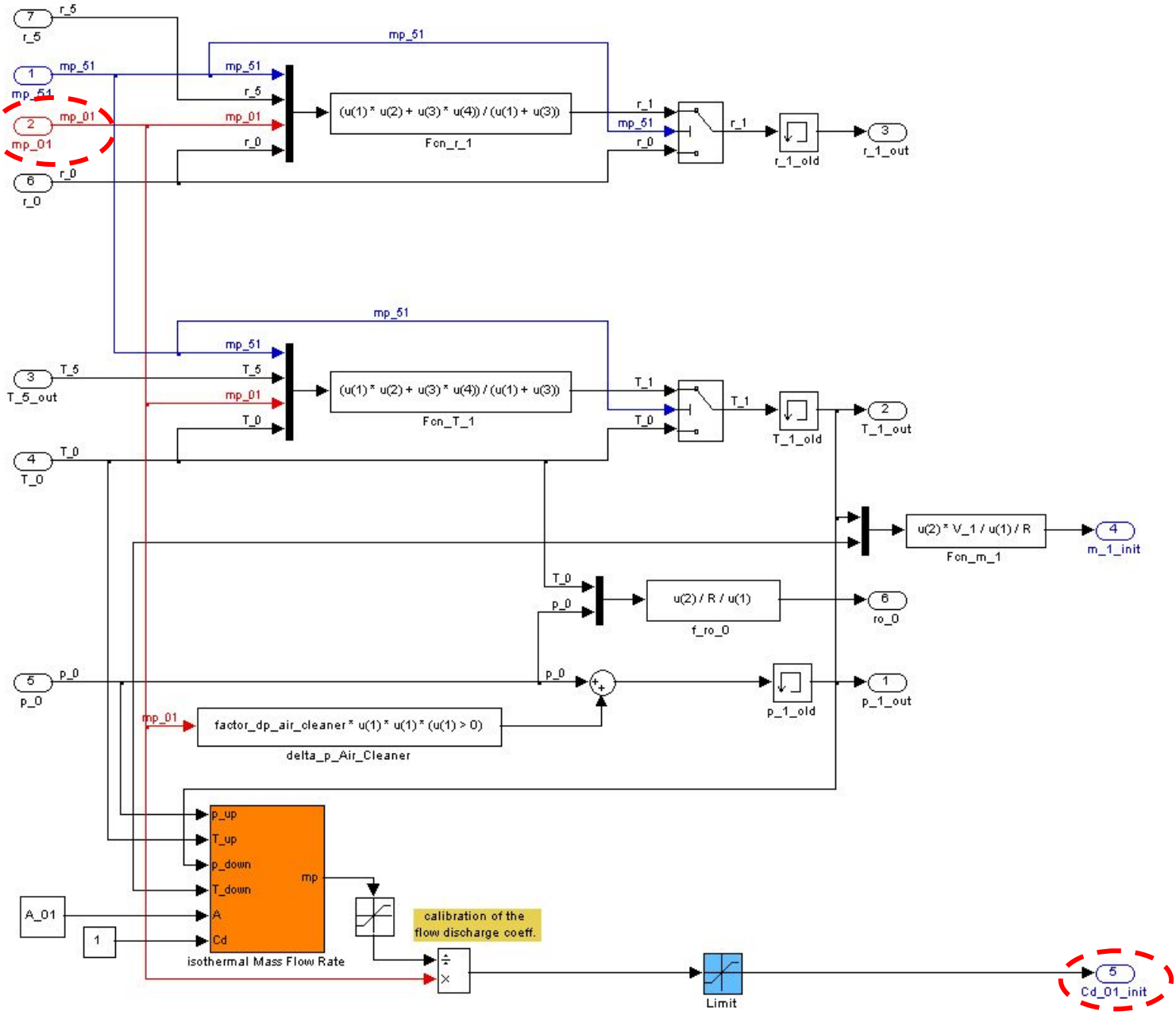

Fig. 8 (zoomed): Air Cleaner submodel from Model_S (go back)

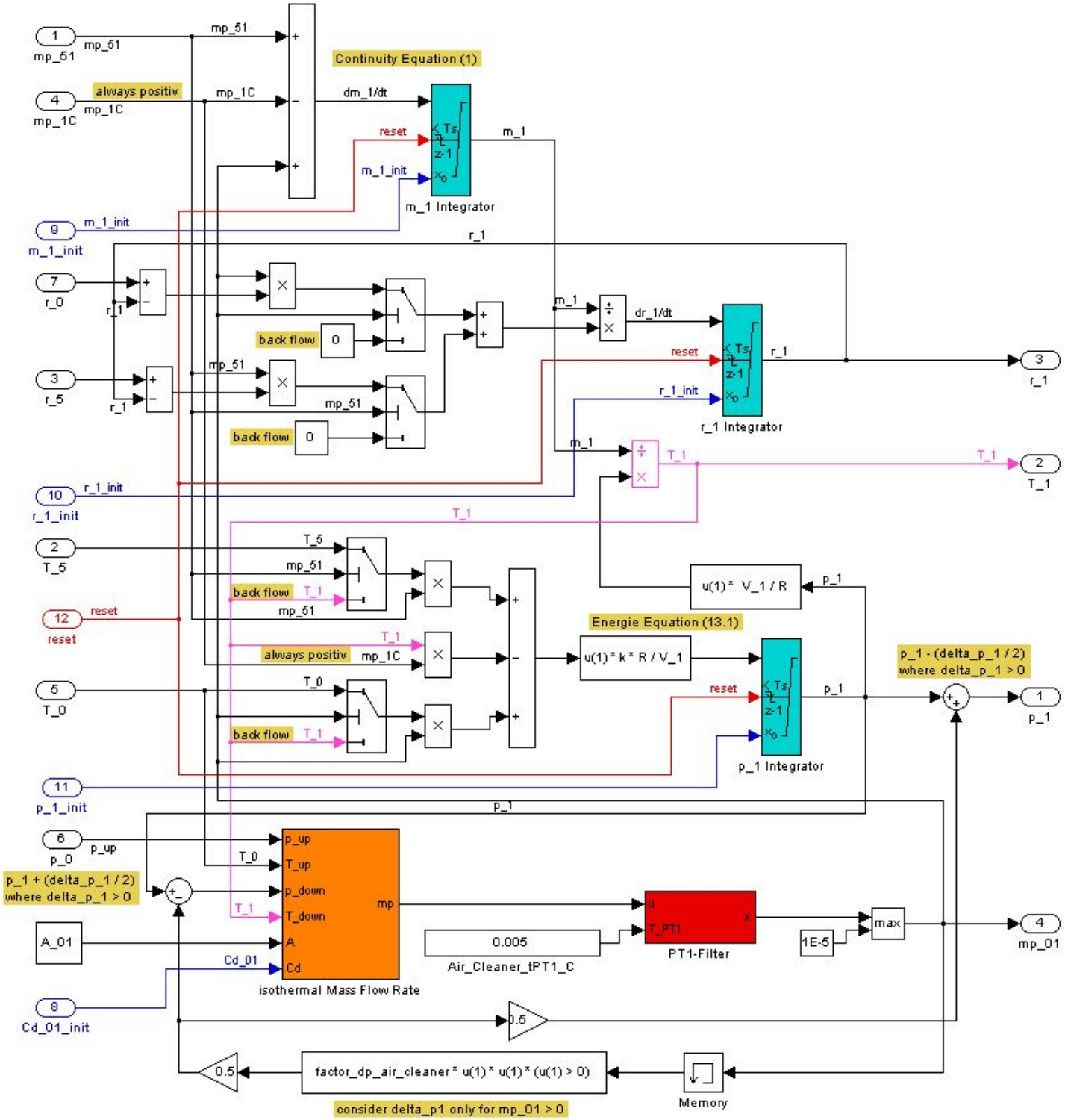

Fig. 9 (zoomed): Air Cleaner submodel from Model_G (go back)